

5 The Reactive extrusion of thermoplastic polyurethane

5.1 Introduction

The kinetics of the polyurethane reaction has been discussed in the previous two chapters. Relevant information on the kinetics was obtained under mixing conditions that also occur during the extrusion process. In the current chapter, we leave the kinetics behind and shift our emphasis to the extruder. As stated in chapter 2, extrusion is a relatively expensive process. Comprehension of the reaction in an extruder, coupled with a rational design of the extruder can therefore lead to a cost benefit. Improvement of the extruder efficiency and control of the product quality may be defined as a goal in that perspective. The efficiency of the extruder operation can simply be expressed as the conversion at the end of the extruder. The product quality is more difficult to grasp, it is related to the conversion, the occurrence of side reactions (allophanate formation, oxidation, crosslinking) and the size and morphology of the hard segments. For the current study the emphasis lies on understanding how the conversion in an extruder can be optimized. The use of an extrusion model is essential, because of the complicated processes that take place in an extruder, and the wide diversity in extruder configurations that are possible. A model can be useful for the optimization of an existing process, the implementation of new types of materials, or the conversion of a batch process into a continuous process.

In the literature, several studies have been directed towards understanding the TPU production in an extruder (1 - 5), each with their own emphasis. Single screw extruders (4, 5), counterrotating extruders (1, 2), and corotating extruders (3) have been studied. A broad range of subjects was covered; predictive modeling (2, 4), reactive blending (3), mixing efficiency in the extruder (1), and the effect of extrusion on product quality (5) are described.

However, a missing subject in this survey is the depolymerization reaction. The depolymerization reaction is inevitably noticeable at temperatures above 150°C (6), which is a typical extrusion condition. The presence of this reaction may hinder the extrusion efficiency. In the current study, the effect of the reverse reaction will be investigated. In addition, the ability of the model to capture the reverse reaction will be examined.

5.2 The Model

5.2.1 Introduction

The purpose of the extruder model is twofold: it should increase the understanding of the complex mechanisms of the reactive extrusion of polyurethane and it should be suitable to optimize the process. In this way, the number of (expensive) experimental trials can be minimized when a new process is designed. To meet this objective, it should be easy to test different extruder configurations and different operating conditions with the model, and the calculation time should be short. In that case, a complex computational fluid dynamics model (CFD-model) is not useful. Therefore, an analytical approach was chosen, which is similar to previous modeling studies (7 -13). Of course, the flexibility and broad applicability of such an engineering model comes with a price. Non-incorporated radial temperature gradients, a simplified approach for the non-Newtonian flow behavior and the complicated flow in the kneading sections may result in a less accurate model prediction.

5.2.2 Reaction

As explained in the introductory section, the main output parameter of the model is the degree of polymerization (α) or the directly related weight average molecular weight (Mw) at the end of the extruder. The degree of polymerization is governed by the reaction kinetics of the polyurethane system under investigation. For this investigation, polyurethane system 2 as described in chapter 4 was chosen. The kinetics of this polyurethane system can be described by a second order rate equation:

$$R_{\text{NCO}} = \frac{d[\text{NCO}]}{dt} = k_f [\text{NCO}]^2 - k_r [\text{U}]$$

$$\text{with } k_f = [\text{Cat}]^m \cdot A_0 \cdot e^{\frac{-E_A}{R \cdot T}}, \quad k_r = \frac{k_f}{A_{0,\text{eq}} \cdot e^{\frac{-E_{A,\text{eq}}}{R \cdot T}}} \quad (2.16)$$

$$\text{and } [\text{U}] = [\text{NCO}]_0 - [\text{NCO}]$$

To predict the isocyanate conversion α in a reactor, the isocyanate balance is solved for that specific reactor, taking into account the above rate equation (equation 2.16). To solve the isocyanate balance, knowledge on the residence time

distribution of the specific reactor is indispensable. Now, for two extreme cases of residence time distribution (no (axial) mixing and complete mixing), the isocyanate balance is solved. Both cases will be used further on in the model.

First, the no-mixing situation is evaluated. Practically, a no-mixing situation is present in a plug-flow reactor. For a plug-flow reactor, the solution of the isocyanate balance, using equation 2.16, is as follows:

$$[\text{NCO}]_N = \frac{(k_r + \sqrt{D}) \cdot C \cdot e^{-t_N \sqrt{D}} + \sqrt{D} - k_r}{2 \cdot k_f \cdot (1 - C \cdot e^{-t_N \sqrt{D}})} \quad (5.1)$$

with

$$D = k_d^2 + 4 \cdot k_f \cdot k_r \cdot [\text{NCO}]_0 \quad \text{and} \quad C = \frac{2k_f[\text{NCO}]_{N-1} + k_r - \sqrt{D}}{2k_f[\text{NCO}]_{N-1} + k_r + \sqrt{D}} \quad (5.2)$$

These equations are also applicable for the conversion in an ideally stirred batch reactor. It is clear from equations 5.1 and 5.2 that the isocyanate concentration is dependent on the residence time and temperature. The concentration at the end of the reactor, $[\text{NCO}]_N$, is expressed as a function of the residence time t_N and the inlet isocyanate concentration, $[\text{NCO}]_{N-1}$.

For the second situation, a completely mixed reactor, the isocyanate balance of a continuous ideally stirred tank reactor (CISTR) can be solved. Since a polymerization reaction is under investigation, the micro-mixing situation in such a reactor is best considered as micro-segregated (14). The conversion in a micro-segregated CISTR is equal to:

$$[\text{NCO}]_N = \int_0^{\infty} [\text{NCO}]_{t,\text{batch}} \cdot E(t) \cdot dt = \int_0^{\infty} [\text{NCO}]_{t,\text{batch}} \cdot \frac{1}{\bar{t}} e^{-\frac{t}{\bar{t}}} \cdot dt \quad (5.3)$$

$[\text{NCO}]_{t,\text{batch}}$ is the isocyanate concentration for a batch reactor with a residence time t , as can be calculated using equation 5.1 and 5.2. Since no analytical solution is available, equation 5.3 is solved numerically in the model.

Obviously, the isocyanate concentration for both reactor types is dependent on the temperature and the residence time. In order to predict the right conversion in the extruder, these parameters must be known. The residence time in the extruder can be extracted from the flow model, while the temperature of the reaction mass along the extruder can be analyzed through the energy balance (which in itself is also

related to the flow model). Furthermore, for every part of the extruder the residence time distribution must be known. All of these issues will be addressed in the following paragraphs. In the concluding paragraph, details on the overall extruder model are given.

5.2.3 Residence time / flow model

In order to be able to predict the residence time, a flow model of the corotating twin-screw extruder is necessary (paragraph 2.2.5). To model the flow behavior in the extruder, it should be taken into consideration that different types of screw elements are used. Most commonly used are the transport elements and the kneading paddles. To introduce the flow behavior in the model, for both element types a simplified approach was chosen, based on the flow between two parallel plates. In this approach, the screw channels are represented as stationary, infinite screw channels, whereas the barrel moves over the channel (paragraph 2.2.1). This approach is similar to previous analytical models (7 - 10, 12, 13). Details on the analysis can be found in these publications. This approach is specifically appropriate for the most commonly occurring elements, the transport elements. For kneading elements, a modification is made to this approach. Both types of elements will be treated separately.

Transport elements

For the transport elements, the filling degree f_T of the not fully filled sections is equal to the ratio of the real throughput (Q) and the maximal obtainable throughput:

$$f_T = \frac{Q}{Q_{S,max,T} - Q_{L,drag}} \quad (5.4)$$

Equation 5.4 is a modified form of equation 2.7. The maximum throughput equals the maximum conveying capacity ($Q_{S,max,T}$) minus the leakage flows ($Q_{L,drag}$) over the flight. The different flows are derived from the parallel plate flow model. Their exact definitions are described by Michaeli et al. (12). Besides the filling degree of the not fully-filled zone, the residence time in a transport section is also determined by the length of the fully filled part. This filled length is a result of the pressure build-up capacity of the element concerned. In case of a larger pressure build-up capacity ($\Delta P/\Delta L$), the (filled) length needed to overcome a pressure barrier is shorter. The pressure build-up capacity in a transport element is calculated according to Michaeli et al. (12) as well:

$$\frac{\Delta P}{\Delta L} = \frac{(Q_{S,max,T} - Q - Q_{L,drag}) \cdot k_{p,T} \cdot \eta_{channel}}{\sin|\varphi| \cdot \left(i \cdot \bar{h}^3 \cdot w \cdot (\pi - \psi) + \frac{w + e}{|\tan \varphi|} \cdot \frac{\delta_R^3 \cdot u \cdot k_{p,T} \cdot \eta_{channel}}{12 \cdot e \cdot \eta_{flight}} \right)} \quad (5.5)$$

$$Q_{L,drag} = u \cdot \frac{V_0}{2} \sin \varphi \cdot \cos \varphi \cdot \delta_R$$

The pressure build up in a transport element is proportional to the viscosity, and to the maximum flow rate minus the real throughput and the leakage flow. The proportionality factor is a function of the channel geometry and a shape factor $k_{p,T}$. The calculation of the maximum conveying capacity ($Q_{S,max,T}$) takes into account the effect of the intermeshing zone. The leakage over the flight is taken into consideration with as well a drag flow dependent ($Q_{L,drag}$) as a pressure flow dependent term (integrated in equation 5.5).

The non-Newtonian behavior of a polymer fluid is taken into account indirectly. The average shear rate in the element is calculated according to Michaeli et al. (10). Both the shear rates over the flight and in the channel are calculated. In order to calculate the shear rate in the channel, a two-dimensional flow analysis is made, for which the actual channel geometry is taken into account. Subsequently, the apparent viscosities are calculated using the appropriate rheological model and the calculated shear rates. This apparent viscosity is used in equation 5.5. In this way, most rheological models can be used.

Kneading paddles

For the kneading paddles, the flow behavior differs considerably from that of a transport element (paragraph 2.2.4). Still, for the current modeling approach, a kneading block is considered as a modified transport element, with an extra leakage flow ($Q_{L,k}$) due to the staggering of the kneading paddles. The maximal conveying capacity is lowered due to this leakage flow. Therefore, the equation to calculate the filling degree of the partially filled zone f_k resembles that of the transport elements:

$$f_k = \frac{Q}{Q_{S,max,K} - Q_{L,drag} - Q_{L,k}} \quad (5.6)$$

In equation 5.6, $Q_{L,k}$ is a result of the extra leakage flow due to the leakage gaps that exists between the staggered kneading paddles. The pressure build up (or consumption) in a kneading section is calculated with (12):

$$\frac{\Delta P}{\Delta L} = \frac{(Q_{S,max,K} - Q) \cdot k_{P,K} \cdot \eta_{channel}}{i \cdot \bar{h}^3 \cdot w \cdot (\pi - \psi)} \quad (5.7)$$

Again, a similarity exists between the equation for the kneading blocks and for the transport elements. The pressure build up in a kneading element is proportional to the viscosity, and to the maximum flow rate minus the real throughput. In case of a kneading element, the extra leakage term due to the staggering of the kneading paddles is incorporated in the equation for $Q_{S,max,K}$. For the kneading blocks, the apparent viscosity is calculated in the same way as for the transport elements.

The approach that is taken in our model for the flow behavior in the kneading blocks suffices for low staggering angles, since in that case, the similarity with the transport elements is still present. However, this model is inadequate at higher staggering angles. In that case, an approach adapted by Verges et al. (13) may give better results. Still, experimental validation of the pressure build up in kneading paddles is scarce. This makes a comparison of the different modeling approaches for the kneading paddles difficult and the present approach sufficient.

5.2.4 Residence time distribution

As explained in the paragraph on the polyurethane reaction, knowledge on the residence time distribution in the extruder is indispensable to calculate the appropriate conversion. In the model, a distinction is made between a kneading block and a transport element, since the flow in a kneading block differs substantially from the flow in a transport element. Moreover, an extra distinction is made between flow in partially filled elements and fully filled elements. In a partially filled element, hardly any axial mixing takes place, because the material is more or less 'glued' to the flank of the screw. Therefore, all the partially filled elements are considered to operate under plug-flow regime, and the isocyanate balance for a plug-flow reactor (equations 5.1 and 5.2) can be used to calculate the conversion in a partially filled zone.

Fully filled transport elements

However, for fully filled elements, the situation differs. In a fully filled transport element, each particle follows a different (helical) path in the screw channel, which causes a distribution in the residence time. Pinto and Tadmor (15) developed a

residence time distribution model, based on this helical flow pattern in the channels of a single screw extruder. This model is also applicable for our self-wiping twin-screw extruder, even though the intermeshing zone will disrupt the flow pattern somewhat. The RTD analysis of Pinto and Tadmor (15) shows that the flow in the fully filled transport elements is neither comparable to plug-flow or flow in a pipe. The actual flow lies somewhere in between. However, as a first approach, the residence time distribution in the fully filled transport elements will be regarded as plug-flow in the current model (equations 5.1 and 5.2).

Fully filled kneading paddles

The flow in the kneading paddles differs completely from the flow in a transport element. In general, in a kneading zone, the circumferential flow rate is much higher than the axial flow rate (16). Besides, due to the squeezing action of two paddles in the intermeshing zone, the mixing is much better. Moreover, a considerable backward flow will be present between two neighboring paddles, because of a leakage gap between these paddles. For these reasons, the residence time distribution in a kneading zone will have a similarity to that of a cascade of continuous ideally stirred reactors. Therefore, this approach is used for the extruder model (equation 5.3). The kneading blocks are divided in a number of CISTR's. Tentative experiments in a Perspex extruder were performed to establish the length of every reactor; it was found to equal half of the screw diameter. This length is typically two to four times the width of a kneading paddle.

5.2.5 Energy

The temperature is the last essential factor that is needed for calculating the conversion in an extruder. The temperature can be derived from the energy balance. In our model, the energy balance for the extruder or for a part of the extruder is:

$$C_p \cdot Q \cdot (T_N - T_{N-1}) = h \cdot A_{\text{wall}} (T_{\text{wall}} - T_N) - Q \cdot \Delta H_R [\text{NCO}]_0 (\alpha_N - \alpha_{N-1}) + W_C + W_F \quad (5.8)$$

The temperature rise in (a part of the) extruder ($T_N - T_{N-1}$) is a result of the heat transfer through the wall, of the exothermic reaction and of the viscous dissipation in the channel (W_C), and over the flight (W_F).

The energy balance considers the extruder or a part of the extruder to be a continuous ideally stirred reactor (CISTR). Obviously, a more complicated flow situation exists in the extruder, which will result in radial and axial temperature

gradients. The latter can be resolved through applying equation 5.8 on short axial sections of the extruder. Nevertheless, the radial temperature gradient can result in a deviation of the measured and predicted temperature in an extruder.

The heat transfer coefficient in the energy balance is adapted from Todd et al. (17). As for the average shear rate in the channel, the viscous dissipation in the channel is calculated using a two-dimensional flow analysis (10). Since the viscous dissipation over the flight is substantial (7), it is integrated in the heat balance according to an equation by Michaeli et al. (10):

$$W_F = \eta_{flight} \cdot \frac{v_0^2}{\delta_R} \cdot i \cdot \frac{e}{\sin \varphi} \cdot \Delta L \quad (5.9)$$

5.2.6 Modeling approach

A general modeling scheme has been developed to calculate the conversion in the extruder. For this calculation, the extruder is split up in segments of a quarter of the diameter of the extruder. The output of the first segment is the input of the second segment and so on. The sectioning is necessary due to the large temperature and conversion gradient in the axial direction. The size that is chosen for the segment is a compromise between accuracy and calculation time.

The sectioning strategy is not compatible with the continuous laminar flow profile that is present in an extruder. For the sectioning approach, a continuous flow is divided into segments that have closed-closed boundary conditions. For example, in case a fully filled transport zone is divided into segments, the residence time distribution over the whole section can be calculated with the approach of Pinto and Tadmor (15). However, to do so for every segment and applying closed boundary conditions will give an erroneous result. To prevent this error, a plug-flow approach is chosen for the transport zones. A plug-flow reactor can be divided in segments without any problems.

Segmental iteration

For a segment N, the temperature T_N , conversion α_N , viscous dissipation W_N , average shear rate γ_N and the viscosity η_N are calculated. The equations used for every parameter are described in the previous paragraph. However, it is not possible to solve these equations sequentially; looking at equation 5.10 it is clear that the equations are interrelated.

$$\begin{aligned}
 \alpha_N &= f(T_N, t_{res,N}, \dots) \\
 T_N &= f(W_N, \alpha_N, \dots) \\
 W_N &= f(\eta_N, \dots) \\
 \eta_N &= f(T_N, \alpha_N, \dots)
 \end{aligned}
 \tag{5.10}$$

Therefore, a dichotomy routine is used to solve equation 5.10 for every segment. The convergence criterion for this routine is the viscosity, since the viscosity is the most sensitive parameter in equation 5.10. In general, the dichotomy routine converged within five steps.

Extruder iteration

Having calculated all variables in segment N, the output of this segment is the input of the next one, segment N+1. However, in an extruder, the situation of this next segment can influence the filling degree of the previous segment. At the start of the ‘extruder iteration’, all segments are considered partially filled. Both the die and reverse or neutral screw elements raise a pressure barrier. This pressure barrier needs to be overcome by the previous segment, which fills ‘itself’ for that reason. A similar mechanism is present in the model (figure 5.1).

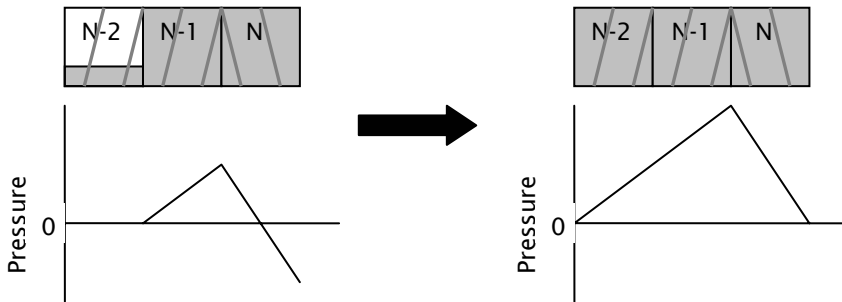


Figure 5.1 The calculation of the filled length in front of a reverse element.

In case a negatively conveying segment (N) is encountered, the upstream segment (segment N-1) is ‘filled’ and recalculated using the segmental iteration. Subsequently, the usual calculation order is followed, so the next (in this case the negatively conveying) segment (N) is calculated. In case the pressure at the end of this segment is still below zero, another upstream segment is filled (N-2) and so on, until the pressure at the end of segment N is zero. For the die, a similar routine is followed. The calculation ends if the pressure at the outlet of the die is atmospheric.

5.3 Experimental section

Several types of experiments were performed to validate the extruder model: cold-flow extrusion experiments, non-reactive extrusion experiments and reactive extrusion experiments. In the experimental section, every type of experiment is addressed separately. Two types of extruders have been used for the validation study: a Perspex extruder ($D = 50\text{mm}$, $Cl = 39\text{mm}$, $\delta_r = 1\text{mm}$, $L/D = 25$) and an APV-Baker MPF50 twin-screw extruder ($D = 50\text{mm}$, $Cl = 39\text{mm}$, $\delta_r = 0.8\text{mm}$, $L/D = 24$). Both extruders can be equipped with different types of transport elements or with kneading paddles (width = $0.25 \cdot D$) with staggering angles of 30, 45, 60, 90, 120, 135 and 150°. For the APV-baker extruder, the temperature of the barrel wall can be regulated through ten independent heating/cooling zones (electric heating, water cooling).

5.3.1 Cold-flow extruder experiments

For the cold-flow experiments, the Perspex extruder was equipped with two-lobed 50/50 (diameter/pitch) transport elements. A calibrated pressure gauge was placed in front of the die and at 22 D. Glucose syrup and a 1.5 % solution of hydroxy-ethyl cellulose (HEC) in water were used for the experiments. Both liquids were rheologically characterized with a constant strain rheometer (TA Instruments, AR 1000-N Rheometer) using a cone and plate geometry. Glucose syrup showed a Newtonian behavior ($\eta = 10\text{ Pa}\cdot\text{s}$) while the shear dependency of the HEC viscosity obeyed a power-law equation ($\eta_0 = 76.1\text{ Pa}\cdot\text{s}$, $n = 0.25$). A gear pump (Maag) was used as a feed pump for the extruder. The throughput was set to 7.5 kg/hour and the rotation speed of the extruder was varied between 12.5 and 100 RPM.

5.3.2 Non reactive validation

Polypropylene (Stamylan PP, DSM) was used for the non-reactive validation. The rheological behavior of the polypropylene was established on the same rheometer as for the cold flow experiments, the rheometer was operated in the oscillatory mode. The temperature dependency of the viscosity could be described with a Williams-Landel-Ferry (WLF) equation:

$$\log\left(\frac{\eta(T)}{\eta(T_r)}\right) = -\frac{C_1(T - T_r)}{C_2 + (T - T_r)} \quad (5.11)$$

With $C_1 = 2.66$, $C_2 = 305.6$, and $T_r = 493$ K. The shear rate dependency was accounted for using the Williamson model:

$$\eta_{\text{app}} = \frac{322.1}{1 + (0.001214 \cdot \dot{\gamma})^{0.625}} \quad \text{at } 493 \text{ K} \quad (5.12)$$

The extruder was equipped with one -45/8/100 kneading zone (stagger angle/number of kneading paddles/ length kneading zone) to ensure complete melting of the polypropylene. The kneading zone was placed 20 cm downstream of the inlet zone. The pressure is measured at three locations for establishing the pressure gradient in the fully filled zone. The temperature is measured in two places along the fully filled zone with non-protruding thermocouples. No significant difference in temperature was observed along the fully filled zone, indicating an isothermal fully filled zone. Five different rotation speeds and five different wall temperatures were investigated. For every experiment, the die diameter was adapted to obtain a sufficiently long fully filled zone. The polypropylene is added to the extruder with a hopper (K-tron T-20). A constant feed rate of 15 kg/hour was maintained.

5.3.4 Reactive validation

Equipment

The extruder layout for the reactive experiments is shown in figure 5.2. One kneading zone (45/8/100) is placed three diameters from the inlet. Only half of the extruder is used for these experiments to prevent an excessive long residence time. Two feed streams are added to the extruder. These streams come together above the feed pocket of the extruder. To premix both streams, a static mixer of the Kenics type of variable length can be placed in the joint feed line. The first stream consists of the premixed chain extender and polyol; the second stream is formed by the isocyanate. A solution of the catalyst in dioctyl-phtalate is added continuously to the polyol feed line using an HPLC-pump. The static mixer of 32 elements is placed after the catalyst injection point to mix the catalyst evenly in the polyol. The isocyanate supply vessel is kept at 25 °C while the polyol supply vessel and feed lines are kept at 80 °C. The flows of both streams are controlled in the same way. A gear pump (Maag TX 22/6) is combined with a flow sensor (VSE, VS-0.04-E) which sends its signal to a PI controller/flow computer (Contrec 802-A). Through a frequency deformer (Danfoss VLT 2010), the PI controller controls the

gear pump. A throughput of 12.5 kg/hour is maintained for most of the experiments.

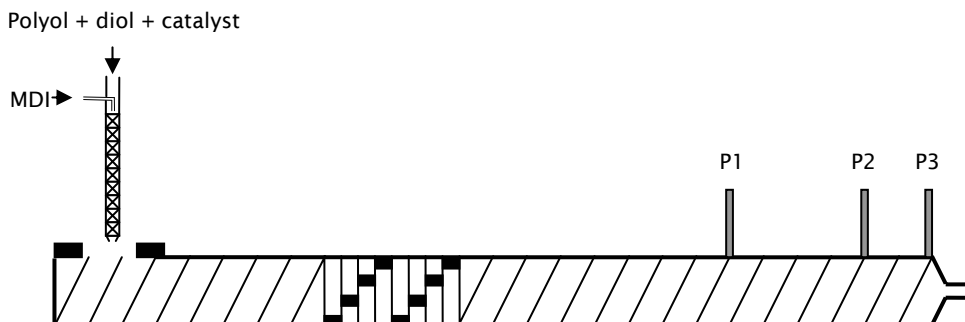


Figure 5.2 The extruder layout for the reactive validation experiments.

Rheo-kinetics

System 2 as described in chapter 4 was used for the reactive extrusion experiments. This system consists of:

- A polyester polyol of mono-ethylene glycol, di-ethylene glycol and adipic acid (MW = 2200 g/mol, $f = 2$).
- Methyl-propane-diol (Mw = 90.1 g/mol, $f = 2$).
- A eutectic mixture (50/50) of 2,4 diphenylmethane diisocyanate (2,4-MDI) and 4,4 diphenylmethane diisocyanate (4,4-MDI). (Mw = 250 g/mol, $f = 2$).

A0, Uncat	(kg/mol s)	$7.4 \cdot 10^4$
EA, Uncat	(kJ/mol)	52.4
A0	(kg/mol-s) · (g/mg)m	$4.53 \cdot 10^7$
m	(-)	2.25
EA	(kJ/mol)	45.18

Table 5.1 The kinetic parameters used for the reactive extrusion model.

Adiabatic temperature rise experiments were used to obtain the kinetic parameters, according to paragraph 6.6.4. For these experiments, the monomers were premixed

with the static mixer as shown in figure 5.2. The resulting kinetic parameters are shown in table 5.1.

As discussed in chapter 4, the reaction rate slows down considerably at high conversions for this polyurethane. Mixing seems to have an effect a high conversions (paragraph 4.4.5), moreover, hardly any catalyst dependence is present (paragraph 4.4.3). Both factors are caused by diffusion limitations. However, the conversion and temperature at which the reaction slows down has not been established. For the extrusion model, a pragmatic approach was chosen to consider the high conversion effects. Above a conversion of 98% ($M_n > 31000$) the kinetics found with the kneader experiment (table 4.1) were applied.

The relationship between viscosity, temperature, and molecular weight has been obtained from the extruder experiments by applying equation 5.13 and 5.14 to the experimental data.

$$k = \frac{P}{\left(2 \cdot \frac{L}{R}\right) \cdot \left(\frac{Q(3 + 1/n)}{\rho \cdot \pi \cdot R^3}\right)^n + C \cdot \left(\frac{Q}{\rho}\right)^n} \quad (5.13)$$

and

$$k = Mw^{3.4} \cdot A_{0,flow} \cdot e^{\frac{U_A}{R \cdot T}} \quad (5.14)$$

In equation 5.14, the consistency of a power-law liquid is given as a function of the molecular weight and temperature (19). Equation 5.13 shows the relationship between the consistency of a power-law liquid k and the pressure drop over the die, with a factor C added for entrance losses. Equation 5.13 can be substituted in equation 5.14. For all different experimental conditions, the pressure drop over the die, the molecular weight, and the temperature of the material coming out of the extruder was measured. In addition, the power law index n of the polyurethane was determined experimentally on a capillary rheometer (Göttfert Rheograph 2003) and found to be equal to 0.61. With these data, a least square fit was performed using a substituted version of equations 5.13 and 5.14, in order to obtain the parameters U_A , $A_{0,flow}$, and C .

5.4 Results

In the result section, a validation study of the extrusion model is presented. Moreover, the effect of several extrusion parameters on the polyurethane extrusion will be discussed and compared with the model. The result section is split into several parts. First, a limited validation study is presented on the pressure build-up capacity of the screw elements. As stated in the theoretical section, a correct prediction of the pressure build-up capacity will contribute substantially to a correct prediction of the residence time and therefore of the end conversion. Moreover, the validity of the approach for the flow model can be tested by checking the pressure build-up capacity. Subsequently the extruder model will be compared to an experimental study on polyurethane extrusion. Measurements on the conversion, temperature, and pressure will be compared with the model predictions. The effect of several extrusion parameters will be discussed and special emphasis will be put on the depolymerization reaction.

5.4.1 Validation of the transport elements, a literature check

As stated in paragraph 2.2.3, the pressure build-up capacity of the transport elements is often expressed as (20):

$$\frac{dP}{dL} = (A \cdot N - Q) \eta \frac{1}{B} \quad \text{or} \quad Q = A \cdot N - \frac{B}{\eta} \cdot \frac{dP}{dL} \quad (2.2)$$

At first sight, a comparison of equation 2.2 with our pressure build up description (equation 5.5) seems troublesome. However, a closer look reveals that the factor B in equation 2.2 is equal to the denominator divided by the k-factor in equation 5.5, while $(Q_{s,max} - Q_{l,drag})/N$ is equal to the A factor. A few experimental studies (21, 22) have been directed to experimental determination of the A and B factors for Newtonian fluids.

D (cm)	Cl (cm)	Pitch (cm)	δ_r (mm)	A (cm ³)	B (cm ⁴)	k (-)
5	3.85	5	0.4	36 / 40.8 [*]	0.12 / 0.118 [*]	27
5	3.85	1.67	0.4	12.8 / 12.4 [*]	0.017 / 0.021 [*]	27
3.07	2.62	2	0.25	4.9 / 4.6 [#]	0.0038 / 0.0045 [#]	27
3.07	2.62	4.2	0.25	9.5 / 11.5 [#]	0.015 / 0.013 [#]	27

Table 5.2 A and B factors for transport elements (bold face current model, * (21), # (22)).

In table 5.2, the results of these studies for transport elements are compared with our model. The resemblance is good, considering the engineering purposes of the model. Strictly speaking, equation 2.2 is only valid for Newtonian fluids. Model calculations show that for non-Newtonian fluids the deviation can be considerable (23), however, no supporting experimental data exists for twin-screw extruders. In literature, some experimental results are shown for which the pressure is plotted versus extruder length for non-Newtonian fluids. We compared one of these studies (8) with our model; the comparison shows a satisfactory agreement (table 5.3).

D=30mm, 28/28	dP/dL (bar/mm) 100 rpm	dP/dL (bar/mm) 200 rpm	dP/dL (bar/mm) 300 rpm
Polystyrene	1.30 / 1.08	1.67 / 1.59	1.88 / 2.0
HDPE	0.78 / 0.65	1.26 / 1.42	1.60 / 1.9

Table 5.3 Pressure build up comparison for non-Newtonian fluids (bold face current model, regular face according to (8))

5.4.2 Validation of the transport elements, an experimental check

As an addition to the literature validation, experiments were performed on a Perspex extruder. In this extruder, the filled length together with the pressure along the filled length can be measured. Sugar syrup was used as a Newtonian experimental fluid. A viscosity of 10 Pa·s was chosen, in order to prevent gravitational effects to be dominant over the viscous forces (24). In addition, a non-Newtonian fluid was tested, which consisted of a 1.5% solution of hydroxy-ethyl cellulose (HEC) in water.

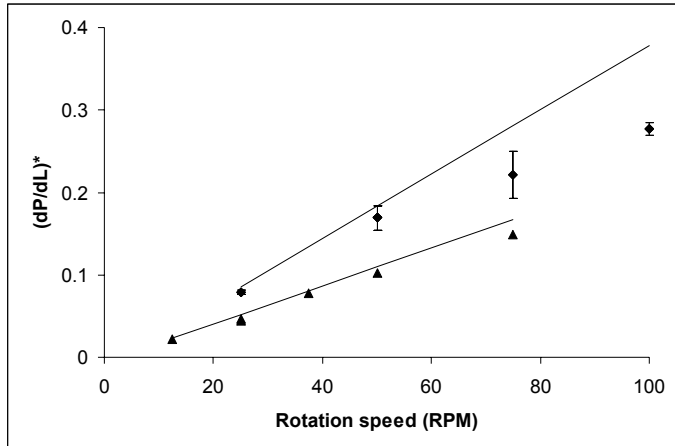


Figure 5.3 The pressure build up capacity as a function of rotation speed. $(dP/dL)^* = (dP/dL) / (\eta_0 \gamma^{(n-1)})$ $D = 5$ cm, $Cl = 3.85$ cm, $pitch = 5$ cm, $\delta = 0.02 \cdot D$, ▲ Hydroxy-ethyl cellulose, ◆ Sugar syrup.

For both liquids, the experimental and model pressure build up capacity of 50/50 transport elements is shown as a function of rotation speed (figure 5.3). The agreement between model and measurement for the HEC is good, while the pressure build-up for the sugar syrup is overestimated at higher rotation speeds. Air bubbles were inevitably present at higher rotation speeds for the sugar syrup experiments, which may cause a deviation of the flow behavior. The pressure build up capacity (expressed as $(dP/dL) / \eta_{app}$) for the sugar syrup is considerably higher than for the hydroxy-ethyl cellulose solution, which is according to expectations. For a non-Newtonian fluid, the apparent viscosity over the flight decreases considerably due to shear thinning. The pressure-driven leakage over the flight is therefore substantially higher than for a Newtonian fluid. Therefore, the pressure build up divided by the apparent viscosity is much lower for HEC than for sugar syrup. These experiments emphasize the importance of the leakage flow over the flight.

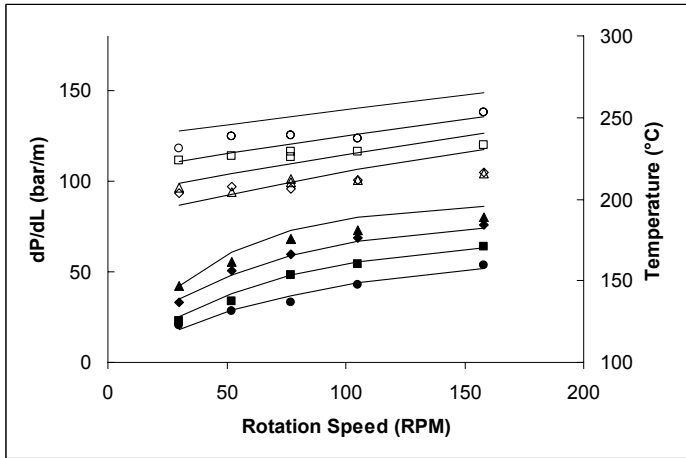


Figure 5.4 The pressure build up and temperature for the polypropylene extruder experiments (barrel wall temperature: ▲190°C, ◆205°C, ■220°C, ●240°C, closed symbols: pressure build up, open symbols: measured temperature).

To test the pressure build up capacity for a non-Newtonian polymeric material, experiments were performed with polypropylene in an APV-Baker twin-screw extruder. The material was rheologically characterized with a cone and plate rheometer. The results of the extruder experiments are plotted in figure 5.4. The pressure build-up capacity is predicted accurately, except for the 190°C experiment. The temperature of the melt seems to be over predicted for all of the experiments. However, the temperature was measured using a wall thermocouple, which tends to underestimate the melt temperature. Since the pressure prediction is correct for these experiments, we can assume the temperature to be predicted correctly. This observation indicates that the energy balance of the model approaches the actual situation.

Considering the validation studies above, the flow in the transport elements is described sufficiently well using the model, at least for the types of transport elements and the extruder diameters that were investigated.

5.4.3 Validation of the kneading elements

Concerning the pressure characteristics of the kneading paddles, less information is present in literature. In an experimental study by Todd (21) the pressure build up characteristics for kneading paddles are expressed in the same A and B factors that are used in equation 2.2. In order to compare these factors with our model, equation 5.7 can be rewritten in a similar manner as was done for the transport

elements. The factor B in equation 2.2 is equal to the denominator in equation 5.7 divided by the k-factor, while $(Q_{s,max})/N$ is equal to the A factor. A comparison between the experiments of Todd (21) and our model is shown in figure 5.5.

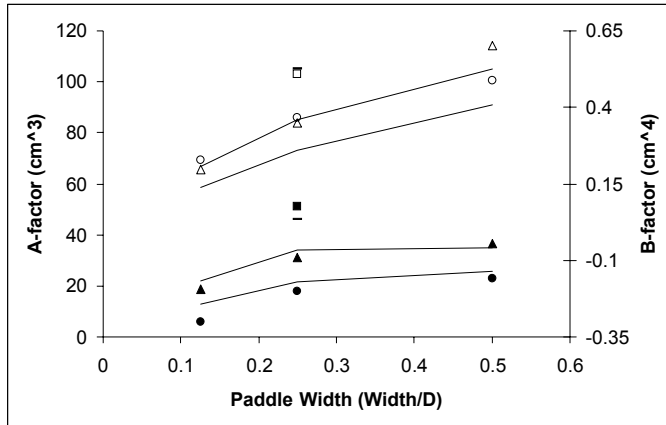


Figure 5.5 A and B-factors for a kneading block as a function of paddle width and staggering angle ($D = 5$ cm, $Cl = 3.85$ cm, $\delta = 0.008 \cdot D$, open symbols B-factor, closed symbols A-factor. Stagger angle: squares 30°, triangles 45°, circles 60°). The lines represent the model simulations, the symbols are the measured values.

In this figure, the paddle width and stagger angle is varied. Considering the simplicity of the modeling approach, the agreement between experiments and model is remarkable. Only for the 60° kneading paddles, the B-factor is largely underestimated. Due to the nature of the modeling approach for the kneading paddles, this deviation is understandable. In the modeling approach, a kneading block is considered as a modified transport element. For larger staggering angles, this approach deviates largely from the actual situation.

For non-Newtonian fluids, hardly any experimental data are present for the kneading elements. With the flow model currently used, Michaeli et al. (12) show a reasonable prediction of the pressure characteristics of the kneading paddles for non-Newtonian fluids. A comparison of the dimensionless pressure build up capacity with a 2-D non-Newtonian model (25) shows an acceptable agreement (figure 5.6). Only for a right-handed 60°-stagger angle element, the pressure consumption is overestimated.

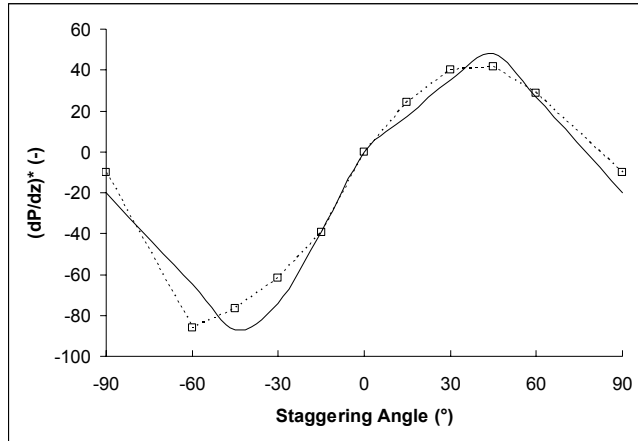


Figure 5.6 Dimensionless pressure gradient $(dP/dz)^* = (\Delta P/\Delta L) \cdot R / (\eta_0 \cdot (2 \cdot \pi \cdot N)^2)$ as a function of staggering angle. The dimensionless throughput $Q^* = Q/(2 \cdot \pi \cdot R^3 \cdot N)$ is equal to 0.05. (solid line = model Noé, dashed line = this chapter).

5.4.4 Polyurethane extrusion

A reactive validation study has been carried out on an APV-Baker MPV-50 extruder. The experimental details of this study are described in a previous section. Obviously, for every experimental setting, a model simulation is generated in order to compare the model prediction with the experiment. Figure 5.7 shows such a simulation for one specific situation. In this figure, the development of the conversion, temperature, pressure, and filling degree along the extruder is shown. Of course, the reaction proceeds mainly in the fully filled sections, due to the longer residence time in these sections. Furthermore, the reaction approaches an equilibrium situation before leaving the extruder; the increase in molecular weight slows down considerably in the last fifteen centimeters upstream of the die. In this area, a dynamic equilibrium is approached for which the forward and the reverse reaction are equally fast. Due to the link between the flow, energy and the reaction, the equilibrium is specific for this particular operation condition and extruder geometry.

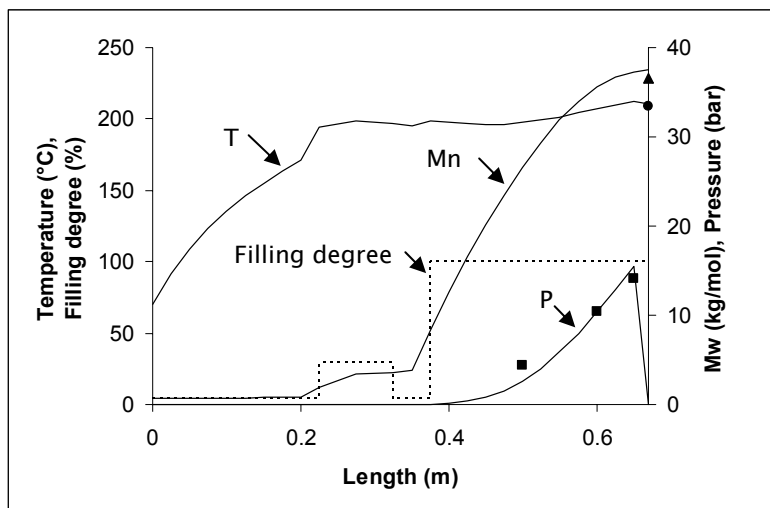


Figure 5.7 An example of the pressure, Mn, temperature and filling degree along the extruder. The number average molecular weight (\blacktriangle), pressure (\blacksquare) and melt temperature (\bullet) at 150 RPM, 12.5 kg/hour, $T_{\text{barrel}} = 185\text{ }^{\circ}\text{C}$, $[\text{cat}] = 30\text{ppm}$, and $d_{\text{die}} = 4\text{ mm}$.

A model simulation as shown in figure 5.7 has been carried out for all operating conditions that were experimentally tested. In order to compare the model with the experiments, the temperature and conversion are preferably measured at different locations along the screw. In this way, a complete view of the extruder performance can be obtained. Furthermore, with these data, a detailed comparison can be made between the model and the experiments. However, in an extruder, the measurement of the temperature and conversion is notoriously unreliable. The temperature of the melt can only be measured using protruding thermocouples, which affects the flow situation considerably (26). Sampling ports are sometimes used for conversion and temperature measurements but they are vulnerable to clogging; moreover, the sampling procedure can take too long for a reliable measurement. To overcome these problems, an inventive and promising sampling port design has been described by Carneiro et al. (27). Unfortunately, such geometry could not be adapted to our extruder. Therefore, our validation study takes into account the conversion and temperature at the end of the extruder. In addition, the pressure development along the extruder is followed by three pressure sensors. The temperature is measured by inserting a thermocouple in the melt coming out of the extruder. The conversion is measured by a size exclusion chromatography method. Material coming out of the extruder is immediately

quenched in liquid nitrogen. Subsequently the molecular weight of the sample is determined as described in chapter 3.

In figure 5.7, the outcome of one extruder experiment is compared with the model. In a similar manner, a wider model validation study has been carried out. For the model validation, the effect of catalyst level, barrel temperature, rotation speed and throughput is investigated. Every variable is discussed shortly in the discussion below.

5.4.5 The effect of the catalyst

In figure 5.8, the effect of the catalyst level on the extruder performance is shown for a barrel wall temperature of 185°C and a rotation speed of 150 RPM. The model predictions and measurements agree reasonably well on the end pressure, outlet melt temperature, and the molecular weight. Due to viscous dissipation, the temperature of the melt exceeds the wall temperature considerably.

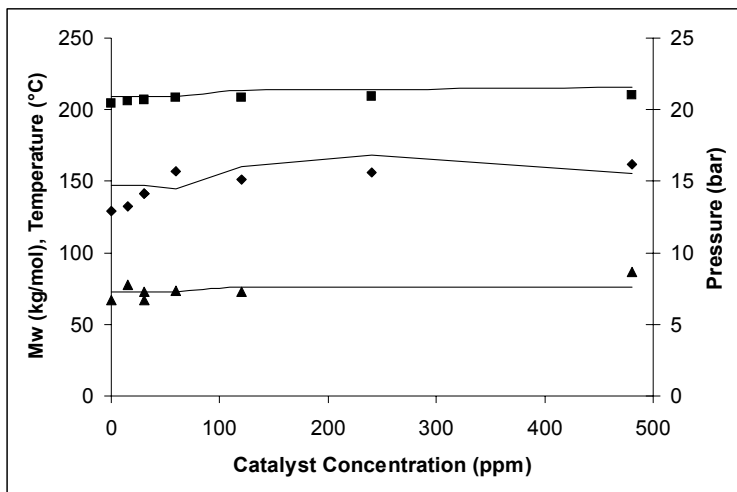


Figure 5.8 Weight average molecular weight (▲), pressure (◆) and melt temperature (■) at the die as a function of catalyst level. (150 RPM, 12.5 kg/hour, $T_{\text{barrel}} = 185^{\circ}\text{C}$, $d_{\text{die}} = 4 \text{ mm}$)

In figure 5.8, a surprising trend is visible; the molecular weight of both the model simulations and the measurements does not show any catalyst dependence. For all catalyst levels, the end conversion and temperature is more or less the same. This observation is not in agreement with earlier kinetic experiments that were performed with this polyurethane (6). In these experiments, a catalyst dependence

was observed. An explanation for the extrusion results may be that the reaction reaches a depolymerization equilibrium before leaving the extruder. In that case, the catalyst concentration has no effect on the end conversion. To test this hypothesis, a more discriminative working zone was tried. The barrel wall temperature was lowered to reduce the effect of the depolymerization reaction. Moreover, we chose a larger die diameter to decrease the residence time in the extruder. The results of these adjustments are shown in figure 5.9.

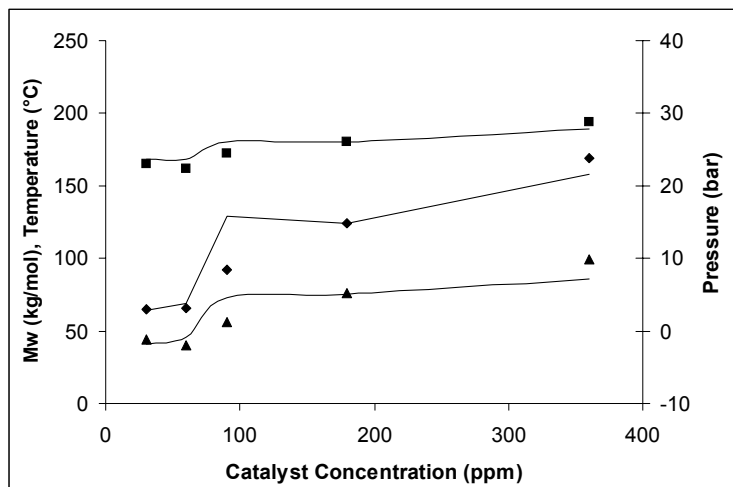


Figure 5.9 Weight average molecular weight (▲), pressure (◆) and melt temperature (■) at the die as a function of catalyst level. (100 RPM, 12.5 kg/hour, $T_{\text{barrel}} = 160^\circ\text{C}$, $d_{\text{die}} = 5 \text{ mm}$)

Clearly, a more profound effect of the catalyst concentration is present for both model and experiment. The agreement between the model predictions and experimental results is reasonable, although a somewhat strange and inexplicable deviation exists at 90 ppm. Nevertheless, the upward trend of molecular weight as a function of catalyst concentration is predicted sufficiently by the model. Remarkably, the catalyst level seems to need a threshold value before having an effect, which can be observed both in the model and experimentally.

5.4.6 The effect of the barrel wall temperature

An increase in the barrel wall temperature is a critical test for the extruder model. Changing the barrel wall temperature has a large influence on the reaction in the extruder, the rheological properties of the polymer and on the heat transfer to the

melt. At a higher temperature, the reaction velocity will increase and the depolymerization reaction will gain importance. Viscous dissipation will have a lesser influence due to a decrease of the viscosity.

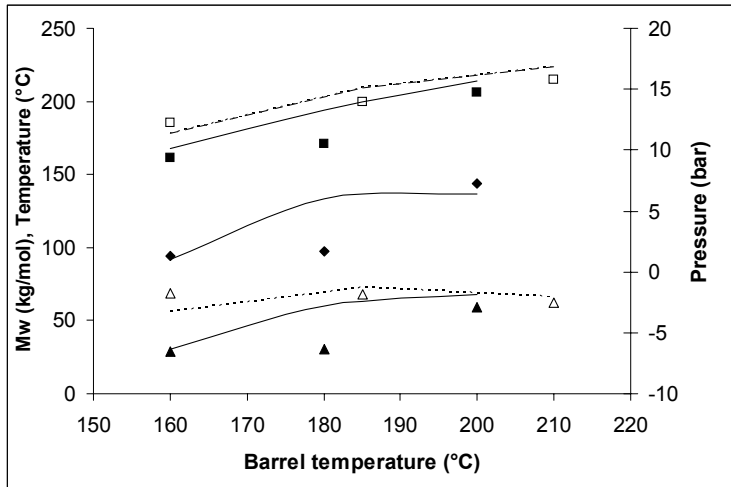


Figure 5.10 Weight average molecular weight (▲), pressure (◆) and melt temperature (■) at the die as a function of barrel temperature. (solid line: 150 RPM, 12.5 kg/hour, [cat] = 30 ppm, $d_{die} = 4$ mm, dashed line (open symbols): 150 RPM, 12.5 kg/hour, [cat] = 30 ppm, $d_{die} = 5$ mm)

The effect of the barrel wall temperature was investigated at two different die diameters. The results are shown in figure 5.10. As can be seen in this figure, the reaction hardly develops at 160 °C and 180 °C for the larger die diameter. At these conditions, the molecular weight at the end of the extruder remains low and viscous dissipation is not present. The latter is clear if we look at the temperature of the melt, which is about the same as the barrel wall temperature. In contrast, at 210 °C, the molecular weight is much higher and approaches its equilibrium value. The combination of residence time and temperature is insufficient to reach a high conversion at lower temperatures. A prolonged residence time or a higher catalyst level will give a better result. The first idea is tested experimentally by decreasing the die diameter. For the current extruder configuration, most of the residence time is generated in the last part of the screw. Therefore, the residence time increases considerably by decreasing the die diameter. As can be seen in figure 5.10, the effect of a longer residence time is considerable at lower temperatures. With a smaller die diameter, the end conversion and temperature of the melt are much

higher at 160°C. This effect lessens at a higher temperature. The decline of the effect of a prolonged residence time at higher temperatures can be attributed to the depolymerization reaction. The depolymerization reaction limits the conversion at higher temperatures. In that case, an increase in residence time does not lead to a higher conversion so that the final conversion for both die diameters is about the same. If this situation were translated to a commercial situation, it would mean that expensive extruder volume is not utilized efficiently, due to the depolymerization reaction.

This paragraph started by stating that an increase in barrel wall temperature is an interesting test for the extruder model. If we now look at figure 5.10, and compare the model and the experiments, the agreement for the small die diameter is reasonably sound. For the larger die diameter, the model prediction does not follow the experiment well at 180 °C. However, the trend going from a low to a high temperature is clearly captured.

5.4.7 The effect of the rotation speed

An increase of the rotation speed has both an influence on the residence time and on the viscous dissipation in an extruder. Due to an increase in the rotation speed, the melt temperature will rise and the residence time will shorten; these effects have an opposite influence on the conversion. Which effect prevails depends on the extruder geometry and the polyurethane under consideration.

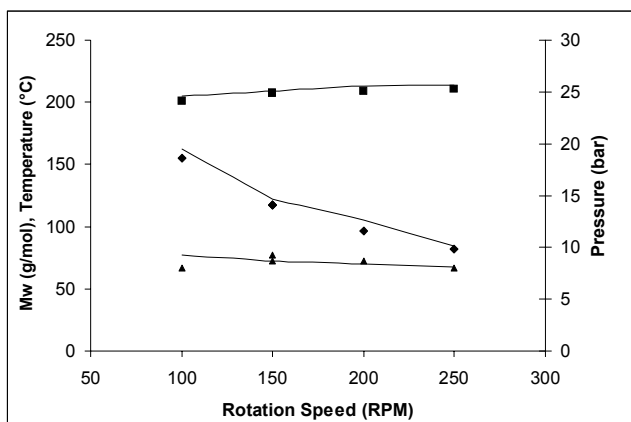


Figure 5.11 Weight average molecular weight (▲), pressure (◆) and melt temperature (■) at the die as a function of rotation speed. ([cat] = 30 ppm, 12.5 kg/hour, $T_{\text{barrel}} = 185^{\circ}\text{C}$, $d_{\text{die}} = 4 \text{ mm}$)

From figures 5.11 and 5.12, it seems that both effects keep each other in equilibrium for this system. In both figures, the rotation speed does not seem to affect the molecular weight to a large extent. As expected, the temperature rises in both situations slightly with increasing rotation speed. However, this effect is not very spectacular and is obviously counterbalanced by a shorter residence time, since the conversion remains approximately the same, independent of the rotation speed. In contrast, the effect of the rotation speed on the end pressure is more obvious. The end pressure decreases with increasing rotation speed. Presumably, the decrease of the end pressure is caused by the combined effect of an increase in temperature and a somewhat lower molecular weight. Both effects lower the melt viscosity and therefore the pressure drop over the die.

If we compare the model with the measurements (figures 5.11 and 5.12), the model follows the experiments well for different rotation speeds. A change in rotation speed gives a change in viscous dissipation and therefore a different equilibrium situation in the energy balance. This means that for the current extruder configuration the viscous dissipation is described sufficiently well.

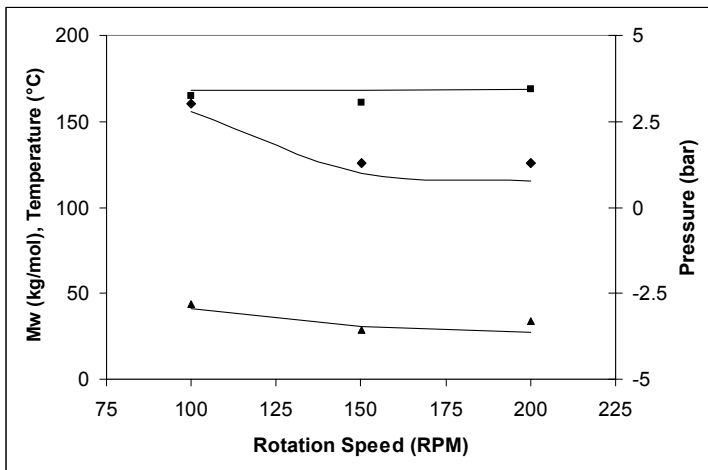


Figure 5.12 Weight average molecular weight (▲), pressure (◆) and melt temperature (■) at the die as a function of rotation speed. ([cat] = 30 ppm, 12.5 kg/hour, $T_{barrel} = 160^{\circ}\text{C}$, $d_{die} = 5\text{ mm}$)

5.4.8 Effect of the throughput

In figure 5.13, the effect of a change in the throughput is shown. Both model and measurement show little effect of the throughput on the molecular weight. A higher throughput will give a higher pressure-drop over the die, which will increase the

filled length in the extruder. However, in this case this increase in reactor volume does not lead to a higher conversion, due to a higher throughput to volume ratio in the extruder. Therefore, the residence time remains more or less constant, giving an equal conversion for all three the throughputs. Figure 5.13 shows that the model prediction for the temperature and conversion is accurate; however, the pressure at the end of the extruder is over-estimated.

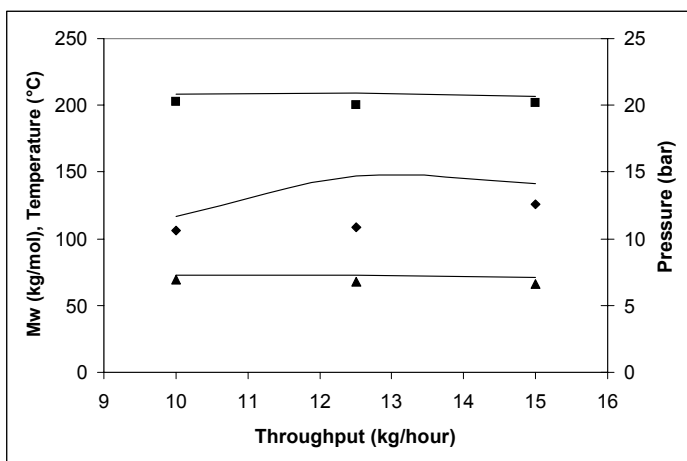


Figure 5.13 Weight average molecular weight (▲), pressure (◆) and melt temperature (■) at the die as a function of the throughput. ($[cat] = 30 \text{ ppm}$, 150 RPM , $T_{barrel} = 160^\circ\text{C}$, $d_{die} = 5 \text{ mm}$)

5.4.9 Depolymerization

Obviously, for all extrusion circumstances, the depolymerization reaction has a severe impact on the extruder performance. Model simulations show that in case the reverse reaction is not incorporated, the simulated molecular weight is a factor ten higher than in case the reverse reaction is incorporated. Likewise, the temperature of the melt is much higher without depolymerization. Of course, for the experiments, the depolymerization reaction cannot be suppressed; the effects of the reverse reaction are always present. In case an experimental parameter is adjusted, the change in molecular weight is dampened by the depolymerization reaction. This effect is very clear for the experiment with different catalyst levels at 185°C . In this case, an increase of the catalyst level does not have any impact, because the reverse reaction limits the maximum conversion. For these experiments, the molecular weight at the die is within five percent of the equilibrium molecular weight at the outlet temperature.

If we focus on this situation, it is somewhat surprising that the conversion reaches almost the same limiting value for every catalyst level. Both model and experiments show this behavior, and for both the model and the experiments, the filled length decreases with a higher catalyst level.

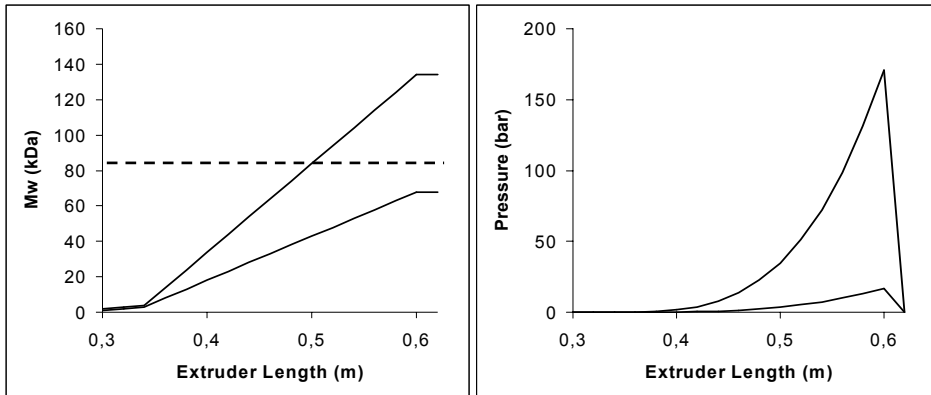


Figure 5.14 Build up of the weight average molecular weight and pressure in front of the die.

If we look at the model, this effect may be explained by the way the filling degree in front of the die is calculated. As described in the theoretical section, the pressure drop over the die must be overcome by the filled length in front of the die. Through an iteration procedure, the filled length is extended from zone to zone until the pressure at the end of the die is atmospheric. If we look at a non-equilibrium second order reaction, the filled length remains more or less the same, independent of the catalyst level, only the conversion increases with an increased catalyst level¹. In figure 5.14, a conceptual (isothermal) drawing of this situation is shown. If a reverse reaction is introduced, the situation changes in figure 5.14. In that case, the molecular weight is limited by, for example, the dashed line in figure 5.14. This means that for the low catalyst run, the situation does not change, regardless of the reverse reaction. However, for the high catalyst experiment, the molecular weight in

¹ For a simplified isothermal situation, the pressure build-up capacity in the filled zones is a function of $Mw^{3,4}$, and the pressure drop over the die is a function of $Mw^{3,4}$. In case the Mw in the filled zone increases (for example due to a higher catalyst concentration), the pressure build up capacity increases. However, the pressure drop over the die rises proportionally, giving an equal filled length. Therefore, for this situation, the reaction velocity does not influence the filled length in front to the die.

the last part of the extruder will not exceed the equilibrium molecular weight. This limitation will result in a lower molecular weight at the die, giving a lower pressure drop over the die. A lower pressure drop will give a shorter filled length upstream of the die and therefore a shorter residence time in the reactor. The result is that the molecular weight is more or less independent of the catalyst level for this situation. Only the filled length changes with the catalyst concentration. Exactly this behavior is observed for the experiments with different catalyst levels at 185°C. The behavior is somewhat different for the experiments at 160°C (figure 5.8). For these experiments, the conversion clearly increases with the catalyst level. Presumably, the conversion for these experiments is lower than the equilibrium molecular weight. In that case, more 'normal' catalyst dependence is observable, which is comparable to the lower curve in figure 5.14. A comparison of the measured weight average molecular weight with the equilibrium molecular weight at the outlet temperature endorses this assumption for the experiments at 160°C. The depolymerization reaction has several important consequences:

- Firstly, the reaction is not finished after a reactive extrusion process. For commercial applications, the polyurethane is pelletized at the die. Due to the equilibrium reaction, the remaining pellets still contain a considerable amount of reactive groups and they will continue to react in the bag. This reaction may continue from hours to days.
- Secondly, the continuous presence in the extruder of reactive isocyanate groups in a pool of urethane bonds may also lead to undesired allophanate formation.
- Thirdly, the depolymerization reaction has a stabilizing influence on the extrusion process. In case the depolymerization reaction governs the extrusion performance, as in the example above, small variations in the process parameters will hardly affect the end conversion. The reaction near the die is very slow, and therefore a small disturbance at the entrance of the extruder will not affect the output to a great extent. However, the obtained extruder stability has a price. Due to the depolymerization reaction, the extruder volume is not used efficiently. Hardly any reaction takes place in the last part of the extruder.

To improve this situation, the throughput can be increased, in combination with a larger die diameter. To evaluate the best combination of throughput and die configuration, the currently developed model can be of use. In addition, the

temperature profile of the extruder may be modified. For example, if the temperature of the zones near the die is lowered, the reaction may proceed to a higher conversion, because the depolymerization reaction is slowed down. Nevertheless, for larger extruders, which operate almost adiabatically, such a measure may not be very effective. Also for this situation, an extrusion model can be helpful to evaluate the net effect.

5.4.10 Pressure build up

For all experiments, the pressure build up characteristics have been measured in the last part of the extruder through three pressure sensors (figure 5.2). The pressure build up capacity in front of the die can be monitored in this way; furthermore, the filling degree in front of the die can be estimated. For reasons of brevity, these data were left out in the foregoing comparison. However, if we compare these data with the model predictions, a clear trend is visible; the model seems to overestimate the pressure build-up capacity in all cases (figure 5.15).

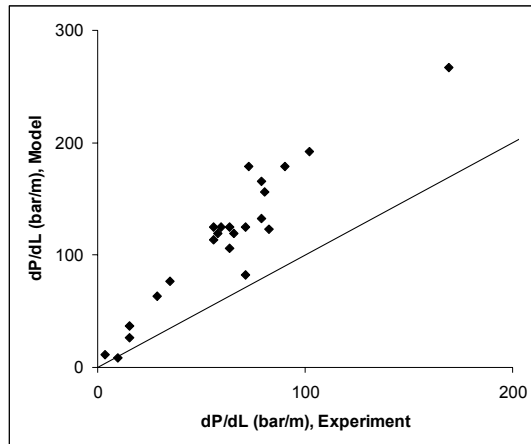


Figure 5.15 Calculated versus measured pressure build up capacity in front of the die.

Several plausible reasons can be formulated for this phenomenon. However, to assess the exact cause of the overestimation of the pressure drop, it is not sufficient to have only data on the pressure drop. Preferably, the conversion along the extruder should also be known. Since the latter could not be determined, the exact reason of the discrepancy cannot be established. Possibly, the k-factor that is used in equation 5.5 is too high, which will result in an over prediction of the pressure build up capacity. On the other hand, the non-reactive validation studies

did not show an inaccurate prediction of the pressure build-up. Another explanation for the discrepancy between model and measurement may lie in the approach for the residence time distribution. The elements in front of the die are considered as plug flow reactors. A plug flow reactor will give a much higher conversion than a well-mixed reactor for the same residence time (14). Therefore, the filled length needed to reach a certain conversion is much shorter for such a reactor. For our specific extruder configuration, it might be expected that the flow behavior in the filled section in front of the die comes closer to a well-mixed reactor than to a plug flow reactor. The extruder is operated at a low throughput in comparison to its maximum throughput capacity. Therefore, in a fully filled section, the pressure flow will almost equal the forward flow, which will lead to considerable back mixing. Moreover, the leakage gap in our extruder is relatively large, which will also contribute to considerable mixing of the material. Both factors contribute to a much higher mixing degree than for a plug flow situation. This will give a lower conversion per centimeter extruder length. Consequently, the experimentally observed pressure drop per length unit is lower than anticipated from the model predictions. A correction factor of 1.3 is applicable in this case.

To improve the residence distribution modeling, a residence time distribution model formulated by Pinto and Tadmor (15), based on the helical flow pattern in the channels of a single screw extruder may be of help. This model is also applicable for a self-wiping twin-screw extruder, even though the intermeshing zone will disrupt the flow pattern somewhat. The residence time distribution (RTD) analysis of Pinto and Tadmor (15) shows that the flow in the fully filled conveying elements falls within plug-flow and flow in a pipe. This observation coincides with the correction factor noticed in the previous paragraph.

In case the RTD approach of Pinto and Tadmor is used in the current extrusion model, it must be incorporated in the 'segmental structure'. The plug flow assumption for transport elements used in the current model prevents difficulties that arise when a continuous laminar flow (as is the case for a screw channel) is subdivided in segments (as is the case for the current extrusion model). In that case, going from segment to segment, closed-closed boundary conditions are unsuitable. In a later stage, this problem will be tackled. To do so, the incoming flow can be divided in a group of small batch reactors that flow through the extruder. In a fully filled conveying zone, every batch reactor will follow a specific continuous path, and have a specific residence time, according to the RTD-function. Going from segment to segment, the flow-lines are not disturbed, so that a batch reactor will have an equal residence time in every segment. For every segment, the conversion of all

batch reactors can be calculated and averaged, to give the average conversion in a segment.

5.4.11 The effect of the residence time distribution on conversion

For a second order reaction, a plug flow reactor is a far more efficient reactor (1.5 to 2 times). In fact, for all n^{th} -order reactions with $n > 1$, a plug flow reactor is more efficient. If only the residence time distribution was important for reactive extrusion, the screw layout should be designed to approach as plug-flow as well as possible. Generally, transport elements are regarded as the screw elements that come closest to plug-flow. The reason that so many other types of elements are used lies in the fact that in an extruder different processes are combined, which require different type of elements.

In process technology, a plug flow reactor is often approached with a cascade of continuous ideally stirred reactors. A similar analogy can be made for extrusion. A study performed by Todd (28) demonstrated that an extruder only filled with kneading elements showed mixing behavior that came closer to a plug flow reactor than an extruder filled with transport elements. However, the forward transport capacity and the energy consumption (and the related temperature rise) with a surplus of kneading paddles may be undesirable. Possibly new types of radial mixing elements (29) may benefit a narrow residence time distribution and improve the efficiency of a reactive extrusion process.

5.5 *Conclusions*

A comparison of the experimental data with the model predictions demonstrates that the present model describes the polyurethane polymerization reaction in the extruder satisfactory, especially considering the engineering approach chosen for the model. The reverse reaction is also captured adequately in the model.

The depolymerization reaction has a profound impact on the extruder performance by limiting the maximum conversion. At the same time, the depolymerization reaction may stabilize the extruder performance due to the considerable decrease of the reaction velocity near the die. Small disturbances at the inlet will be wiped out at the fully filled reaction zone near the die. From an extruder performance point of view, this stagnant zone is an inefficient use of expensive reactor volume. In addition, the consequence of the reverse reaction is that polyurethane that exits the extruder may continue to react in the bag. A prolonged presence of a polymerization-depolymerization equilibrium may be disadvantageous due to the possible occurrence of side reactions (e.g. allophanate formation).

The depolymerization reaction is an extra complicating factor for understanding polyurethane extrusion. An extruder model is therefore a helpful tool for optimizing the polyurethane extruder.

The current approach for the residence time distribution in the model is coarse. For example, at the relative high pressure to drag flow ratio that is present in the current extruder configuration, the residence time distribution in the filled transport elements comes closer to ideally stirred than to plug flow, while the latter approach is used in the model. However, a correction factor can be used in this case.

5.6 List of symbols

A_0	Reaction pre-exponential constant	mol/kg · s
$A_{0,flow}$	Flow pre-exponential constant	Pa · s ⁿ
A_{wall}	Surface of the barrel wall	m ²
C	Correction for entrance losses at the die	1/m ^{3·n}
C _p	Heat capacity	J/kg · K
[Cat]	Catalyst concentration	mg/g
e	Flight land width	m
E_A	Reaction activation energy	J/mol
$E_{A,eq}$	Equilibrium reaction activation energy	J/mol
E(t)	Exit age function	-
f	Functionality	-
f_t	Filling degree of a not fully filled transport element	-
f_k	Filling degree of a not fully filled kneading element	-
h	Height of the screw channel	m
h	Heat transfer coefficient	J/s · m ² · K
i	Number of channels	-
k	Power law consistency	Pa · s ⁿ
k_0	Forward reaction rate constant, catalyst independent	mol/kg · s
k_{eq}	Equilibrium reaction rate constant	mol/kg
k_f	Forward reaction rate constant, catalyst dependent	kg/mol · s
$k_{p,t}$	Shape factor for transport elements	-
$k_{p,k}$	Shape factor for kneading elements	-
k_r	Reverse reaction rate constant	1/s
L	Length of the die	m
m	Catalyst order	-
M_w	Weight average molecular weight	g/mol
n	Reaction order	-
n	Power law index	-
N	Rotation speed	1/s
[NCO]	Concentration isocyanate groups	mol/kg
$[NCO]_0$	Initial concentration isocyanate groups	mol/kg
$[NCO]_N$	Isocyanate concentration at the outlet of a reactor	mol/kg
$[NCO]_{N-1}$	Isocyanate concentration at the inlet of a reactor	mol/kg
$\Delta P/\Delta L$	Pressure gradient in the axial direction of the extruder	Pa/m

Chapter 5

Q	Throughput	kg/s
$Q_{S,max,T}$	Maximum conveying capacity, transport elements	kg/s
$Q_{S,max,K}$	Maximum conveying capacity, kneading elements	kg/s
$Q_{L,drag}$	Drag term of leakage flow over the flight	kg/s
$Q_{L,k}$	Leakage flow between the kneading paddles	kg/s
R	Gas constant	J/mol K
R	Radius of the die	m
R_{NCO}	Rate of isocyanate conversion	mol/kg·s
t	Time	s
T	Temperature	K
u	Circumference of the eight-shaped barrel	m
[U]	Concentration urethane bonds	mol/kg
U_A	Flow activation energy	J/mol
v_0	Circumferential velocity of the screw	m/s
V	Volume ATR reactor	m ³
w	Width of the screw channel	m
W_C	Viscous dissipation in the channel	J/s
W_F	Viscous dissipation over the flight	J/s

Greek symbols

α	Conversion $(1 - [NCO] / [NCO]_0)$	-
δ_R	Clearance between barrel and flight tip	m
$\dot{\gamma}$	Shear rate	1/s
$\eta_{channel}$	Viscosity in the channel	Pa · s
η_{flight}	Viscosity over the flight	Pa · s
ψ	Intermeshing angle	-
φ	Pitch angle	-

5.7 References

1. K.J. Ganzeveld, and L.P.B.M. Janssen, Polym. Eng. Sci., **32**, 457 (1992).
2. A. Bouilloux, C.W. Macosko and T. Kotnour, Ind. Eng. Chem. Res., **30**, 2431 (1991).
3. P. Cassagnau, T. Nietch and A. Michel, Int. Polym. Process., **14**, 144 (1999).
4. M.E.Hyun and S.C. Kim, Polym. Eng. Sci., **28**, 743 (1988).
5. G. Lu , D.M. Kalyon, I. Yilgör and E. Yilgör, Polym. Eng. Sci., **43**, 1863 (2003).
6. V.W.A. Verhoeven, A.D. Padsalgikar, K.J. Ganzeveld and L.P.B.M. Janssen, J. Appl. Polym. Sci. , accepted for publication
7. H.E. Meijer and P.H.M. Elemans, Polym. Eng. Sci., **28**, 275 (1988).
8. H. Potente, J. Ansahl and R. Wittemeier, Int. Polym. Process., **3**, 208 (1990).
9. H. Potente, J. Ansahl and B. Klarholz, Int. Polym. Process., **9**, 11 (1994).
10. W. Michaeli, A. Grefenstein and U. Berghaus, Polym. Eng. Sci., **35**, 1485 (1995).
11. H.Kye and J.L. White, Int. Polym. Process., **11**, 129 (1996).
12. W. Michaeli, and A. Grefenstein, Int. Polym. Process., **11**, 121 (1996).
13. B. Vergnes, G. Della Valle and L. Delamare, Polym. Eng. Sci., **38**, 1781 (1998).
14. K.R. Westerterp, W.P.M. Van Swaaij and A.A.C.M. Beenackers, Chemical Reactor Design and Operation, John Wiley & Sons, New York, Brisbane, Chichester, Toronto (1984).
15. G. Pinto and Z. Tadmor, Polym. Eng. Sci., **10**, 279 (1970).
16. H. Potente, Untersuchung der Schweissbarkeit Thermoplastischer Kunststoffe mit Ultraschall, Aachen (1971).
17. D.B. Todd, SPE ANTEC Tech. Papers, **34**, 54 (1988).
18. V.W.A. Verhoeven, M.P.Y. Van Vondel, K.J. Ganzeveld, L.P.B.M. Janssen, Polym. Eng. Sci., **44**, 1648 (2004).
19. D. W. Van Krevelen, Properties of Polymers, Elsevier, Amsterdam (1990).
20. L.P.B.M. Janssen, Reactive Extrusion Systems, Marcel Dekker Inc., New York, Basel, (2004).
21. D.B. Todd, Int. Polym. Process., **6**, 143 (1991).
22. T. Brouwer, D.B. Todd and L.P.B.M. Janssen, Intern. Polym. Process., **17**, 26 (2002)
23. Z. Tadmor, G. Gogos, Principles of Polymer Processing, John Wiley & Sons, New York, Brisbane, Chichester, Toronto (1979).
24. R.A. De Graaf, D.J. Woldringh, and L.P.B.M. Janssen, Adv. Polym. Tech., **18**, 295 (1999).
25. J. Noé, Etude des écoulements de polymères dans une extrudeuse baxis corotative., Phd-thesis, Ecole des Mines Paris (1992).
26. M.V. Karwe and S. Godavarti, J. Food Sci., **62**, 367 (1997).
27. O.S. Carneiro, J.A. Covas and B. Vergnes, J. Appl. Polym. Sci., **78**, 1419 (2000).
28. D.B. Todd, Chem. Eng. Prog., **69**, p. 84 (1969).
29. D.B. Todd, Plastic compounding, Hanser, Munich (1998).

